High-resolution seismic profiling in the Sea of Marmara (northwest Turkey): Late Quaternary sedimentation and sea-level changes

A. D. Smith *Bullard Laboratories, Madingley Rise, Cambridge, CB3 OEZ, England*
T. Taymaz, **F. Oktay** } *İ.T.Ü. Maden Fakültesi, Jeofizik Müh. Bölümü, 80626-Maslak, İstanbul, Turkey*
H. Yüce, **B. Alpar**, **H. Başaran** } *Hydrographic Service, Turkish Navy*
J. A. Jackson *Bullard Laboratories, Madingley Rise, Cambridge, CB3 OEZ, England*
S. Kara, **M. Şimşek** } *Hydrographic Service, Turkish Navy*

ABSTRACT

High-resolution sparker seismic profiling was carried out in the Sea of Marmara (northwest Turkey) to study the late Quaternary tectonics and sedimentation of this important active basin at the western end of the North Anatolian fault zone. A sedimentary unit interpreted as the clinoforms of a prograding delta was observed in places along the outer part of the southern shelf. The topset-foreset transitions of the latest clinoforms cluster around 100 m below present sea level; they were probably deposited during the last glacial maximum and early phase of deglaciation, between 25 and 13 k.y. B.P., when the level of the Aegean was below that of the Dardanelles sill (60–70 m below sea level at present). Therefore, the Sea of Marmara was isolated from the Aegean during the last glacial maximum, but it is possible that a fluvial overflow existed across the Dardanelles during this time, stabilizing the level of the "Marmara Lake" and allowing the delta progradation. Rivers that drain into the Sea of Marmara from the south have a much greater combined drainage basin area and sediment flux than those draining the region to the north. This may explain the much broader shelf to the south: half graben bounded by north-dipping normal faults observed within the southern shelf would tend to trap sediment sourced from the south and subdue any sea-bed morphology on the shelf.

INTRODUCTION

The Sea of Marmara is a marine basin in northwest Turkey that connects the Aegean Sea with the Black Sea. It is 275 km long and 80 km wide with a broad shallow shelf to the south and a series of deep (up to 1250 m) subbasins to the north (Fig. 1). The Sea of Marmara is located at the western end of the North Anatolian fault. Across most of Turkey the North Anatolian fault is a relatively simple, narrow, right-slip fault zone; however, it splits into several fault strands in the vicinity of the Sea of Marmara so that the deformation becomes distributed over an ~120 km broad zone (Fig. 2, inset; Barka and Kadinsky-Cade, 1988; Şengör and others, 1985). The distributed deformation continues to the west across the North Aegean (Taymaz and others, 1991). Numerous damaging earthquakes have affected the Sea of Marmara region in historical time (Ambraseys and Finkel, 1991; Ambraseys, 1988). Both strike-slip and pure normal faulting earthquakes have occurred in the region (Taymaz and others, 1991).

The Sea of Marmara is connected to the Aegean Sea by the Dardanelles (Çanakkale) strait, which has a present-day sill depth of 60–70 m, shallower than the lowest recorded (−115 m to −118 m) fossil shorelines in the Aegean (van Andel and Lianos, 1984). Therefore, sea-level oscillations during late Quaternary time (Chappell and Shackleton, 1986) must have been a major control on the paleogeography and stratigraphy of the Sea of Marmara. It is likely that during the last lowstand, the Sea of Marmara was isolated from the Aegean and, hence, the global ocean system (see Stanley and Blanpied, 1980). The relative altitudes of the Dardanelles sill and the Aegean Sea during the last lowstand, however, will not be the same as the present-day relative altitudes of the fossil shorelines and the Dardanelles sill because of the isostatic response of the lithosphere to the postglacial transgression (Lambeck and others, 1990).

In this paper, we examine the relative contributions of tectonics and glacio-eustatic sea-level changes in controlling the morphology of the sea bed and the patterns of late Quaternary sedimentation and erosion in the Sea of Marmara. The database includes high-resolution sparker seismic reflection profiles combined with Turkish Petroleum Company (TPAO) multichannel seismic reflection profiles and detailed bathymetric data (from the Turkish Navy Hydrography Service).

Five hundred kilometers of 1 kJ analog sparker profiles were collected in the Sea of Marmara during September/October 1988 on the Turkish Navy ship *T.C.G. Çubuklu* (Fig. 2). The sparker data were recorded directly onto paper, usually to 200 ms TWT (two-way time), and imaged the top 100 m or so of the subsurface.

GSA Bulletin; August 1995; v. 107; no. 8; p. 923–936; 12 figures.

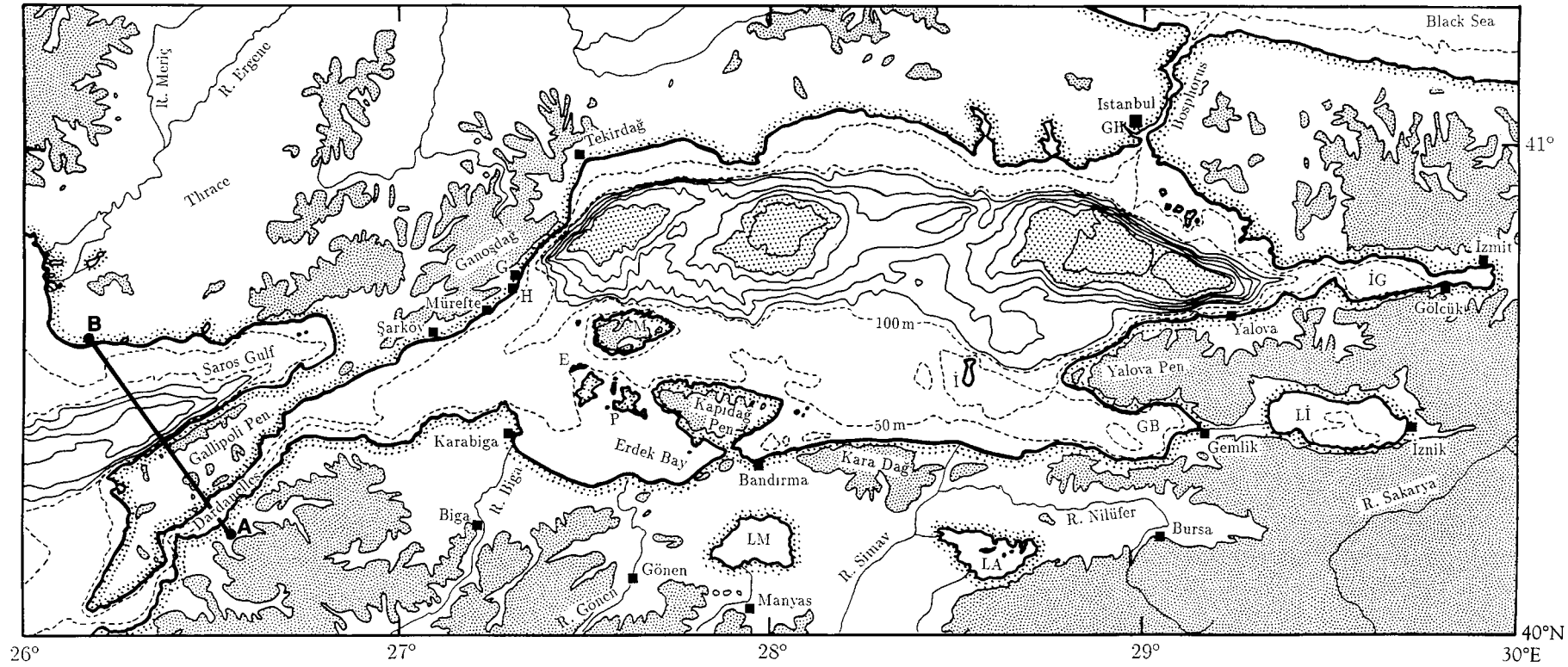

Figure 1. Bathymetric and topographic map of the Sea of Marmara region. The bathymetry is taken from unpublished Turkish Navy data, Admiralty charts, and IOC-UNESCO maps. Below sea level, the bathymetric contours with intervals of 200 m are drawn as solid lines; the dashed lines are the 50 m and 100 m bathymetric contours. Topography above 200 m is stippled. The map also gives the location of geographical features mentioned in the text: E, Ekinlik Island; G, Gaziköy; GB, Gemlik Bay; GH, Golden Horn; H, Hoşköy; İ, İmralı Island; İG, İzmit Gulf; LA, Lake Apolyont; Lİ, Lake İznik; LM, Lake Manyas; M, Marmara Island; P, Paşalimanı Island. The location of the bathymetric profile in Figure 9a across the Gallipoli peninsula is marked A–B.

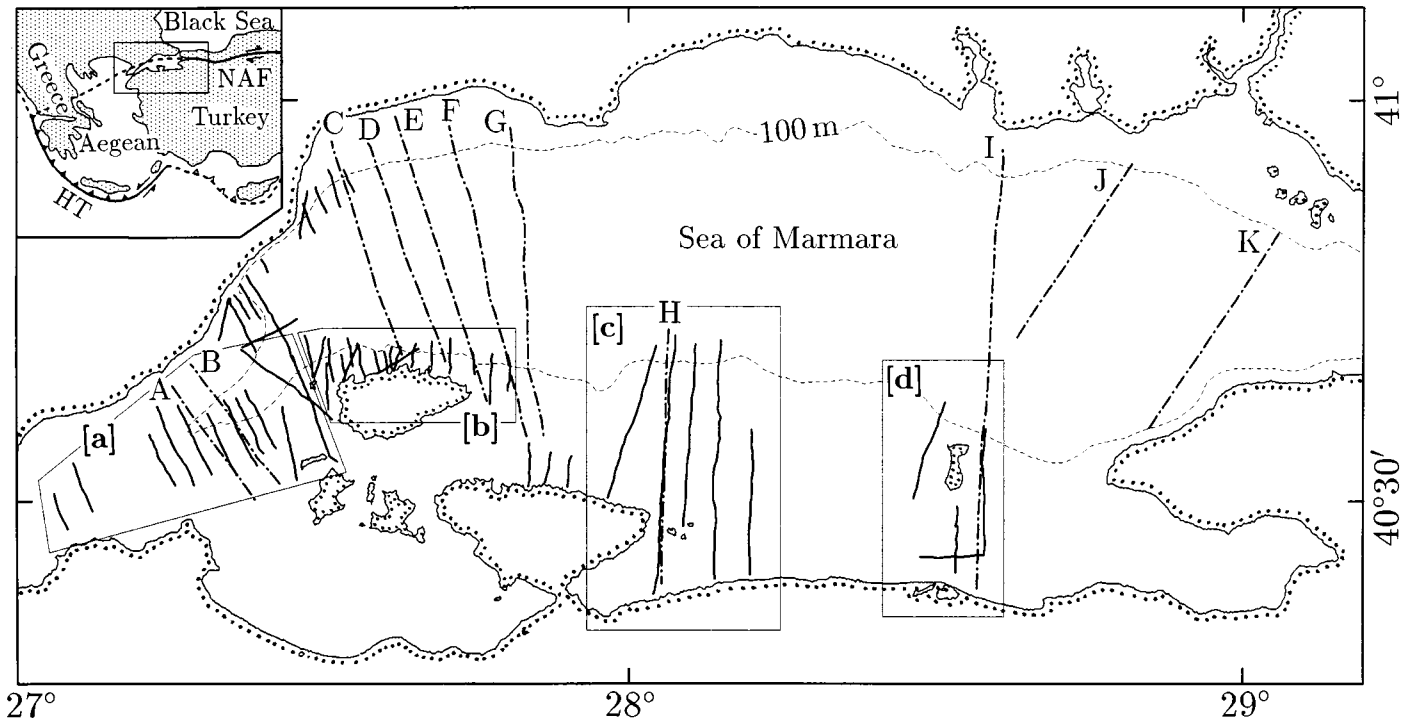

Figure 2. Track chart showing the location of the sparker survey profiles (solid lines), and selected Turkish Petroleum (TPAO) multichannel seismic reflection profiles (broken lines labeled with capital letters A through K) in the Sea of Marmara. The lettered polygons delimit the subregions, which are described separately in the text. The dashed line is the 100 m bathymetric contour. The rectangle within the inset is the location of the study area. The North Anatolian fault (NAF) is marked as a continuous line east of the Sea of Marmara, but to the west across the Sea of Marmara and the North Aegean, the faulting becomes distributed (schematically represented by the dashed line). HT, Hellenic Trench.

The data were generally of good quality in shallow regions, but they deteriorated abruptly in areas of steep sea-floor gradients and deeper water. This paper concentrates mainly on the southern shelf region. The analog sparker data are affected by the reverbatory nature of the source wavelet (bubble pulse). This is apparent in the reflectors from the sea bed (Fig. 3). Therefore, caution is necessary in geologic interpretations of the data. Navigation was by Trisponder, using three shore-based radio beacons with an accuracy of about 10 m. To estimate reflector depths we use 1750 ms^{-1} as a reasonable approximation of average sediment velocities. The multichannel data we examined were in the form of unmigrated time sections recorded to 4–6 s TWT; they were used primarily to identify which of the structures seen on the sparker profiles are major structures at depth. Sparker profiles are hereafter referred to by the prefix MAR- and the multichannel data by TPAO-.

SEISMIC STRATIGRAPHY

The shallow seismic reflection data set has few intersecting profiles, and cross-correlation is therefore difficult. It is sometimes possible to correlate among profiles using prominent reflectors and distinctive sequences of reflectors, and on this basis a seismic stratigraphy has been established for the southern shelf region. The stratigraphy is briefly described here (Fig. 3); the rationale behind the tentative dating of the units is given later in the paper.

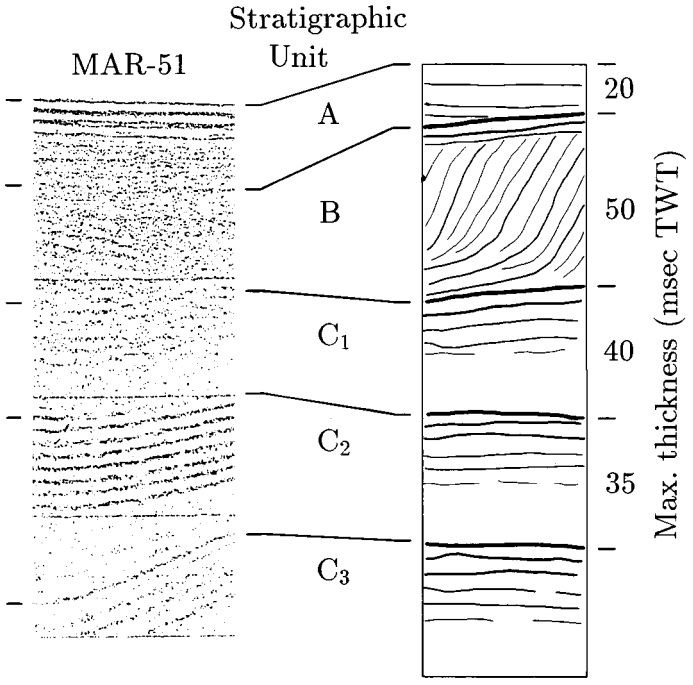

Figure 3. A synthetic representation of the seismic stratigraphy together with an example of real sparker data (from MAR-51, see Fig. 8).

Stratigraphic Unit A

The uppermost unit varies from 0 to 20 ms TWT (0–18 m) thick. It seems to drape older units, and we interpret it as a Holocene posttransgression marine deposit.

Stratigraphic Unit B

This unit is up to 50 ms TWT (≈45 m) thick and, in some profiles, is separated from the overlying unit by a strong reflector, which is a low-angle unconformity. It is easily recognized on many profiles near the shelf break by its basinward-prograding reflectors or clinoforms with a sedimentary dip of about 10°; however, identification of the unit is difficult where the clinoforms are absent. In some profiles, there is a lateral transition from the clinoforms to flat-lying parallel reflectors. We interpret the clinoform seismic facies as prograding deltaic sediments, deposited at a time of stable or gradually falling base level, probably during the last glacial maximum and early phase of deglaciation (25–13 k.y. B.P.) when the Sea of Marmara was a lake isolated from the Aegean.

Stratigraphic Unit C

This unit consists of a series of subunits with flat-lying, parallel, continuous reflectors, bounded by strong reflectors. The layering within each subunit appears to be stronger in the upper part than in the lower part, which is transparent in several profiles, but in some cases this may be an artifact of the bubble pulse. Each of the subunits on a particular profile has a similar thickness, between 17 and 40 ms TWT (15–36 m). We interpret them as subaqueous sediments, deposited during an oscillating base level, and probably of late Pleistocene age, younger than the 135 k.y. B.P. sea-level lowstand. Where the prograding clinoform facies of unit B is absent, the upper subunit of unit C may be confused with unit B.

DESCRIPTION OF AREAS

Because the shallow seismic profiles cluster into separate areas, we describe the details of these areas separately (Fig. 2).

Approaches to the Dardanelles (Çanakkale Straits)

Southeast of Mürefte and Şarköy (Figs. 1 and 4c), the sea bed of the Sea of Marmara in the approaches to the Dardanelles has the form of a gently sloping shelf (in the depth range 60–90 m), bounded at its lower margin, the shelf break, by a steeper dipping (≈7°) slope and at its upper margin by a steeper coastal slope. The depth of the shelf break varies between 90 and 104 m, a range ubiquitous throughout the Sea of Marmara. The scarp slopes define a central channel that deepens toward the northeast, toward the westernmost of the (>1000 m) deep-water basins; to the southwest, the channel morphology diminishes and disappears as the shelf shallows (Fig. 1).

There is a high density of sparker profiles in this region (subregion [a] of Fig. 2). The upper unit (stratigraphic unit A) on the southern shelf is thin (<20 ms TWT) in Figure 4b. This unit is less clearly distinguished in Figure 4a. The top of stratigraphic unit B is defined by the reflector R_1; it is a unit up to 45 ms TWT (≈40 m) thick, within which incoherent reflected energy dominates. Some steeply dipping reflectors or clinoforms are imaged within this unit, which dip north at about 15° (Fig. 4b). The clinoforms are absent southeast of fault F_3, where the equivalent unit is much thinner. Reflector R_2 separates the clinoforms of stratigraphic unit B from stratigraphic unit C, which is composed of units of subhorizontal reflectors bounded by stronger reflectors.

We interpret the clinoforms as the deposits of a prograding delta. Because the water depth to the foreset-topset transition was controlled by wave base (probably about 10 m; Aksu and others, 1987), this unit was deposited when the relative level of the Sea of Marmara was significantly lower than today; the delta probably formed at the contemporaneous mouths of the Gönen and Biga Rivers (Fig. 1). Aksu and others (1987) described very similar units, though of a larger scale, from shallow seismic reflection profiles in Izmir Bay, offshore western Turkey; they interpreted the units as deltaic deposits. The prograding clinoform facies of stratigraphic unit B is also present on the margins of the northern shelf, but it is of insignificant volume and extent compared to the equivalent deposits on the southern shelf. This northern shelf is largely an erosional feature with only a thin veneer of undeformed sediments (Fig. 5).

Fault F_3 cuts the sea bed with an apparent normal offset of 3 m down to the north (Fig. 4a) and, therefore, has been recently active. This fault may be traced across several adjacent sparker profiles and the multichannel profiles, striking at 260°, and is at least 11 km long.

North of Marmara Island

Marmara Island, like the Kapıdağ Peninsula and the other smaller islands on the south side of the Sea of Marmara (Fig. 1), is composed of granitic intrusions and metamorphic rocks (M.T.A., 1964). On the north side of Marmara Island, metamorphosed limestone and dolomite form an indented coastline.

North of the island is a 2- to 5-km-wide shelf bounded by the shelf break at about 95 m depth. Numerous short sparker profiles traverse this narrow shelf (subregion [b] in Fig. 2). The shelf in this subregion may be divided into two areas on the basis of morphology: a back-tilted (0.2° to the south) terrace-like area to the west, and a gentle basinward sloping shelf to the east. On profiles northwest of Marmara Island (Fig. 6b) the sea bed of the shelf is underlain by a unit of reflectors that dip north at 5°–9° and flatten with depth. We correlate this unit with the clinoforms seen in the Şarköy subregion (stratigraphic unit B) because they closely resemble each other and are at similar altitudes (the top of the foresets in Fig. 6b are 92 m below sea level). Below the clinoforms in Figure 6b are subparallel reflectors that dip gently north (stratigraphic unit C). Across the narrow shelf north of Marmara Island, the clinoforms of stratigraphic unit B decrease progressively in height then disappear from west to east, concomitantly with the transition of the shelf morphology from the back-tilted terrace to a gentle north-dipping slope (Fig. 6).

The sea-bed gradients in the slope region north of the shelf break are typically 10°–20°. The sea-bed morphology is highly irregular, as revealed in sparker and multichannel profiles, and between the shelf break and the basin plain are north-south–trending canyon-like features (Fig. 1). These observations suggest that the slope region is dominated by slumping and other mass gravity transport processes, which are to be expected on steep sedimented slopes in a seismically active basin. There is no direct evidence in the reflection data for an active fault north of Marmara Island, along

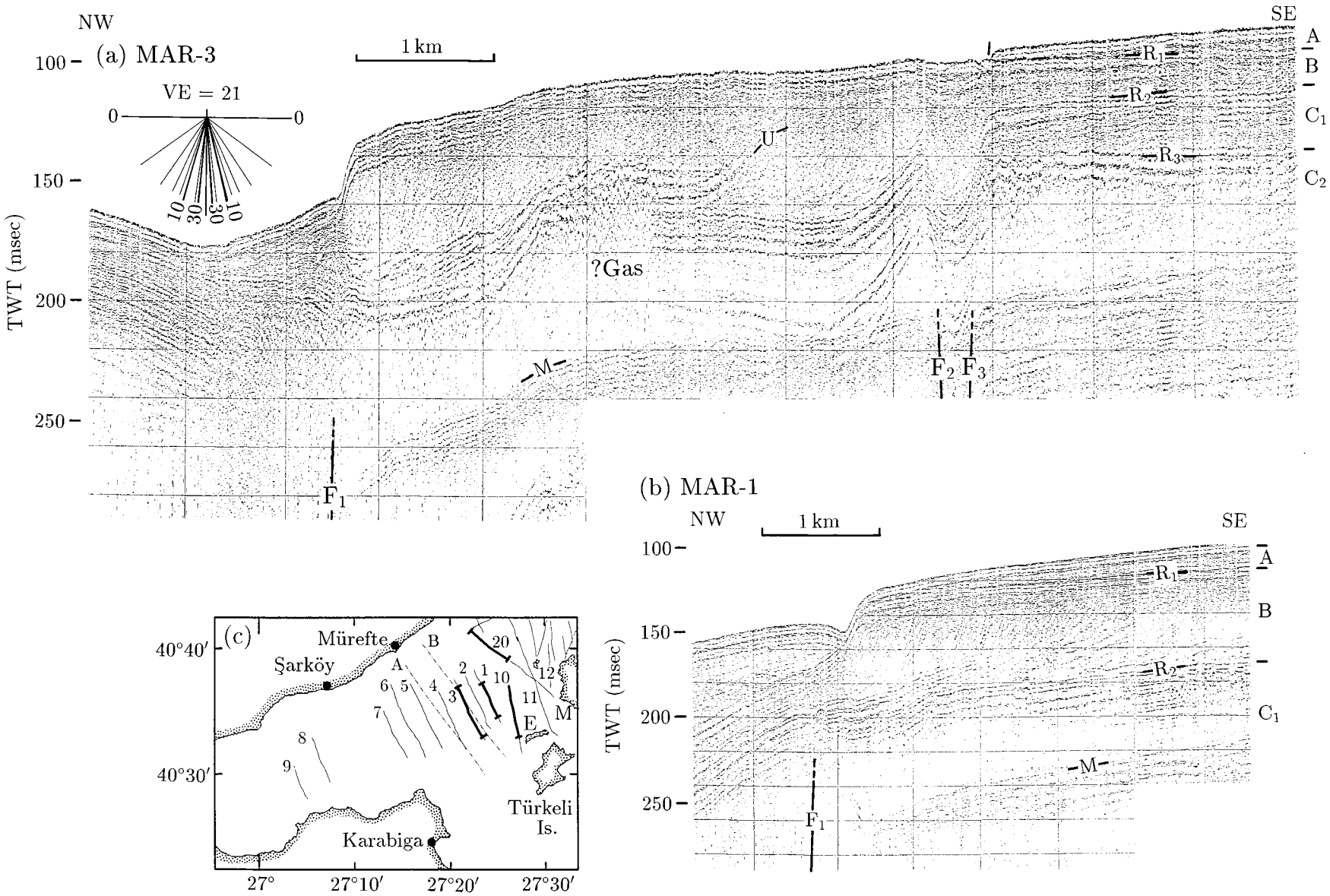

Figure 4. Sparker profiles from the Şarköy subregion (subregion [a] on Fig. 2). (a) Part of sparker profile MAR-3. The slope angle nomogram on this and other sparker profiles is constructed using a sea-water seismic velocity of 1500 ms^{-1} and the average speed of the ship along the profile (which varies slightly); therefore it is approximate. On this and all following sparker profiles, M is the first sea-bed multiple; $R_{1,2...}$ are prominent reflectors; $F_{1,2...}$ are faults; and A, B, $C_{1,2...}$ refer to stratigraphic units (see Fig. 3). (b) Part of sparker profile MAR-1. (c) Location map of the Şarköy subregion: Sparker profiles are marked by continuous lines; the segments of the profiles shown in (a), (b), and MAR-20 in Figure 5 are marked by thicker lines; TPAO multichannel profiles are shown as broken lines. E, Ekinlik Island; M, Marmara Island; VE, vertical exaggeration.

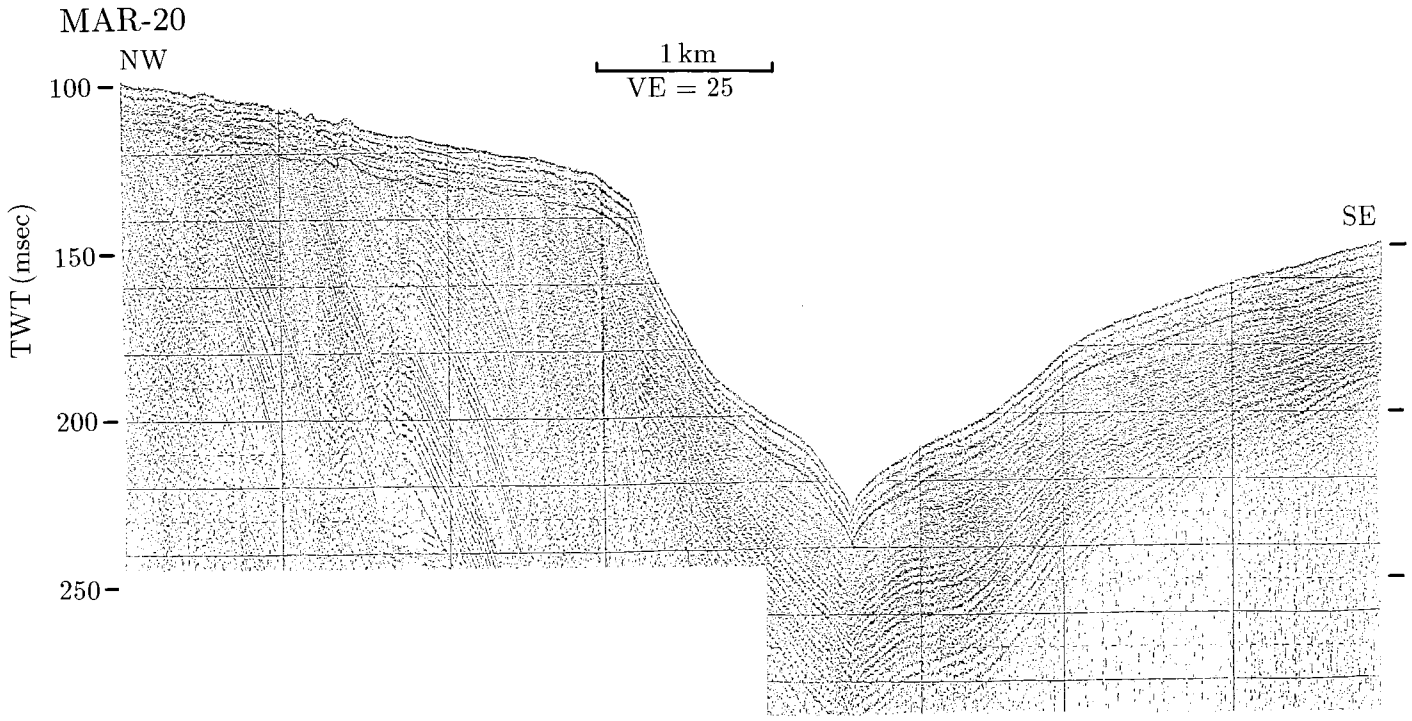

Figure 5. Sparker profile MAR-20, showing the central channel and northern shelf in the Şarköy subregion. For the location of this profile, see Figure 4c.

either the coast or the shelf break, but data quality is poor on the steep slopes north of the shelf break, and any active faults may have been obscured by slumping.

East of the Kapıdağ Peninsula

The area east of the Kapıdağ Peninsula (subregion [c] in Fig. 2) is a very gently sloping (av. 0.2°) shelf up to 32 km wide, with a depth of 50 m close to the shore and 100 m at the shelf break in the north. The data include one multichannel seismic reflection profile, recorded to 4 s TWT, and 5 parallel sparker profiles, the longest of which closely follows the track of the multichannel profile (Fig. 7d).

The multichannel profile TPAO-H (Figs. 7b and 7c) crosses two half grabens bounded by north-dipping faults. Continuous dipping reflectors from the half-graben fill are observed down to about 2.0 s TWT. The major faults are also observed in the sparker data (Fig. 7a), where they cut reflectors just below the sea bed but are not associated with sea-bed scarps. In the hanging wall of the major fault F_5, a wedge of recent sediments and reflectors dip toward a syncline in the hanging wall. Fault F_6 is as prominent as fault F_5 in the sparker profile (Fig. 7a), but it is not resolved in the multichannel profile (Fig. 7c) and so must have a relatively small displacement.

Faults F_7 and F_8 have large (≈100 ms TWT) offsets on the sparker records but are not resolved in the multichannel data. Being close to the shelf break, they may be slump scar faults and therefore only superficial features. It is unclear from the poor-quality seismic reflection data near the shelf break whether or not a major basin-bounding fault is present along the shelf break in this region.

In contrast to the subregions to the west, the prograding clinoform facies of Stratigraphic Unit B are not observed on sparker profiles in this subregion. It is therefore difficult to correlate the reflectors within the hanging wall of fault F_5 (Fig. 7a) with those south of the shelf break in the Marmara Island and Şarköy subregions. Much of the southern shelf was probably subaerially exposed or above wave base during the progradation of the clinoforms because, at present, the base of stratigraphic unit A in the hanging wall of fault F_5 is at least 20 m higher than the foreset-topset transition of the observed clinoforms at the shelf break. Therefore, stratigraphic unit B may be absent or thin here, in which case the prominent reflectors R_1 and R_2 probably bound the subunits of stratigraphic unit C.

Faults that cut the surficial sediments on the shallow seismic reflection profiles commonly have no or only subtle bathymetric expressions, even if they are associated with major faults seen in the multichannel data. For example, fault F_5 has no sea-bed scarp in Figure 7a, although a shoal whose long axis is parallel to the strike of the fault is located in its footwall (defined by the 50 m bathymetric contour northeast of the Kapıdağ Peninsula in Fig. 1). The absence of sea-bed scarps may be explained by coastal or subaerial erosion of fault scarps during periods of lower sea (or lake) level and concomitant sedimentation in the adjacent half-graben basins. There has probably been little fault displacement, however, since the Holocene marine transgression.

İmralı Island

The north-south multichannel profile east of İmralı Island (subregion [d] in Fig. 2; TPAO-I in Fig. 7d) indicates that the island is the emergent crest of a tilted block bounded by a large normal fault on its northern side. Surface geology and geomorphology support this interpretation: The steep north side of the island consists of Upper Cretaceous rocks (M.T.A., 1964) and is onlapped from the

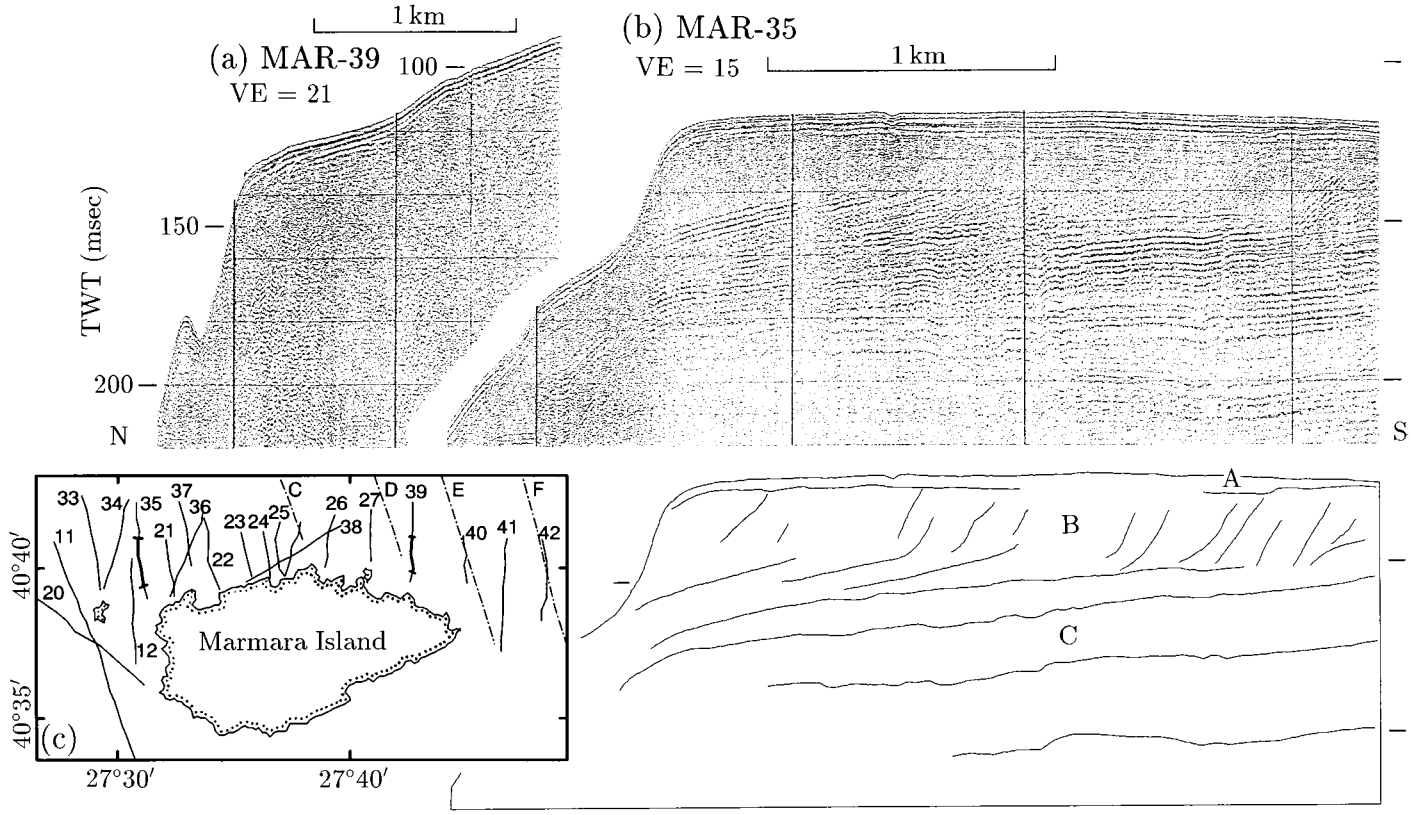

Figure 6. (a) Part of sparker profile MAR-39, northeast of Marmara Island. (b) Part of sparker profile MAR-35, northwest of Marmara Island, below which is an interpretation of the profile. A, B, and C correspond to the stratigraphic units of Figure 3. (c) Location map of profiles north of Marmara Island (subregion [b] on Fig. 2). The segments of the profiles in (a) and (b) are marked by thicker lines.

south by Neogene strata dipping gently south at about 7°. The southern part of the island has a subdued topography. İmralı Island is located on a broad shoal, well defined by the 50 m bathymetric contour (see Fig. 1). The north side of this shoal is straight and trends at 276°, connecting with the western tip of the Yalova Peninsula.

The southern part of the sparker profile 3 km west of İmralı Island (Fig. 8) has planar, parallel reflectors dipping south at about 8°, unconformably overlain by flat-lying reflectors. The dipping reflectors on the sparker profile may be correlated with the Neogene sediments on İmralı Island.

In the northern part of the sparker profile (Fig. 8), a series of fault scarps cut the sea bed and downthrow prominent reflectors to the north. The faults show syn-sedimentary growth and sea-bed scarps, and offsets of the prominent reflectors are progressively smaller toward the north; the southernmost fault has the largest offset with a 7-m-high sea-bed scarp. These faults are the surface expression of a major north-dipping normal fault bounding a 3.0 s TWT deep half graben, which is observed on the coincident multichannel profile (not shown here). The shelf break is located at the northern end of Figure 8.

Below the upper 20 ms TWT (stratigraphic unit A) is a unit of north-dipping reflectors that thickens abruptly to the north, as concomitantly the dips of the reflectors steepen (stratigraphic unit B). This unit resembles that seen in the Şarköy subregion and northwest of Marmara Island, and the fossil slope break (the topset-foreset transition of the northern limit of the unit) is at a similar depth (105 m below sea level); we interpret it as a unit of prograding, probably deltaic, coastal deposits. Below stratigraphic unit B are a series of alternating strong parallel reflectors and almost transparent units (stratigraphic units C_1, C_2, and C_3). Hence the complete stratigraphy in Figure 3 is present in the profile.

SEA LEVEL AND DATING

Late Quaternary Sea Level

Lacking any direct evidence as to the age of the sediments observed in the sparker survey, we have attempted to correlate the stratigraphy with published sea-level curves for the late Quaternary (Chappell and Shackleton, 1986; Fairbanks, 1989). The ICE-3G deglaciation model of Tushingham and Peltier (1992) predicts that the relative sea-level curve for the eastern Mediterranean during the last 15 k.y. closely follows the well-determined curve for Barbados, based on the dating of coral terraces (Fairbanks, 1989; recalibrated using Th/U dating by Bard and others, 1990). In a high-resolution seismic profiling survey offshore from the southern Argolid in the Aegean, van Andel and Lianos (1984) found the lowest glacial shorelines at −115 m to −118 m, close to the lowest point on the Barbados curve. According to these curves, the maximum rates of sea-level change are greater than typical tectonic subsidence or sedimentation rates when averaged over $\sim 10^3$ yr. Therefore, at a par-

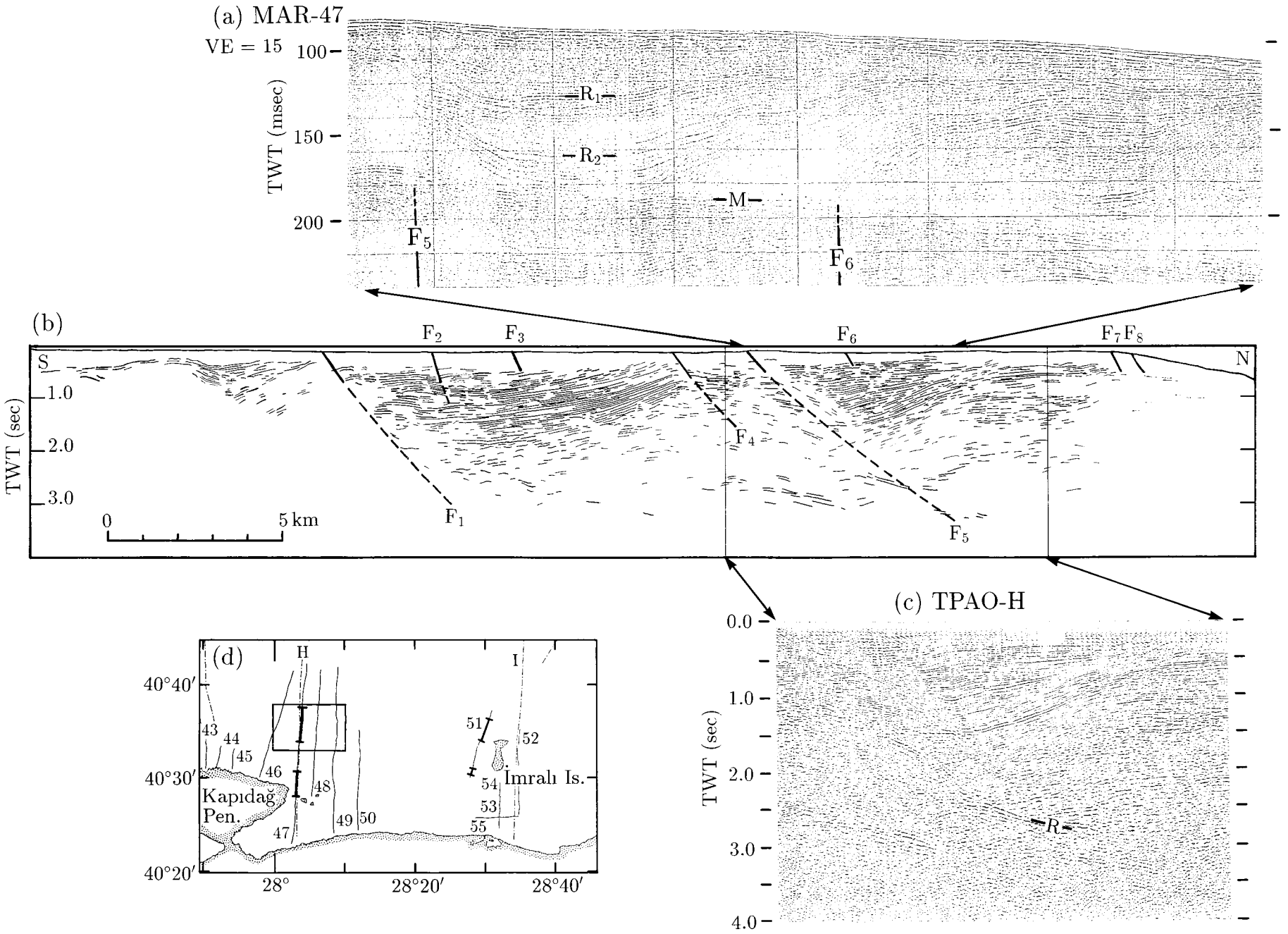
(a) MAR-47
VE = 15
TWT (msec)
100
150
200
R1
R2
M
F5
F6
(b)
F2
F3
F6
F7F8
S
N
TWT (sec)
1.0
2.0
3.0
0
5 km
F1
F4
F5
(c) TPAO-H
TWT (sec)
0.0
1.0
2.0
3.0
4.0
R
(d)
H
I
40°40′
40°30′
40°20′
28°
28°20′
28°40′
43
44
45
46
47
48
49
50
51
52
53
54
55
Kapıdağ
Pen.
İmralı Is.

Figure 7. Seismic reflection profiles from the subregion east of the Kapıdağ Peninsula. (a) Part of sparker profile MAR-47. (b) Line drawing of the multichannel profile TPAO-H, with faults identified from the sparker data. Those faults that correspond to major faults seen in the multichannel data are extended downward as dashed lines; however, their geometry is not well constrained. (c) Part of the multichannel profile TPAO-H, from which the line drawing in b was derived, showing the northernmost of the two half grabens along this profile. (d) Location map of the subregions east of the Kapıdağ Peninsula [c], and near İmralı Island [d] (Fig. 2). Sparker profiles are shown as continuous lines, and TPAO multichannel profiles are shown as broken lines.

ticular location, a major control on the stratigraphy should be sea-level oscillations.

Today the Sea of Marmara connects the Aegean Sea (and via the Mediterranean, the world ocean system) with the Black Sea. Both connections, the Dardanelles to the Aegean and the Bosphorus to the Black Sea, are narrow, shallow marine straits: The present-day maximum depth of the Dardanelles is about 60–70 m, whereas the Bosphorus has a maximum sill depth of <40 m. That a similar situation also existed during previous sea-level highstands is testified by the marine pulses observed in Black Sea DSDP cores (Schrader, 1979); however, this chronostratigraphy is based on a correlation of the marine pulses with the northern European glacial-interglacial stratigraphy, so the ages of the highstands are not independently determined.

If we wish to know whether the Sea of Marmara was isolated from the Aegean during the last glacial maximum, then we need to know the relative levels of the Dardanelles sill and the Aegean at that time. This will not be the same as the present-day relative altitudes of the Dardanelles sill and the lowest glacial shorelines in the Aegean because of the isostatic response of the lithosphere to the postglacial sea-level rise. Because of the physiography of the region, the spatial variation of this water load was irregular and flexural effects are potentially important. The flexural isostatic response of the lithosphere to the postglacial sea-level rise may be estimated using the expressions for the deflection of a continuous elastic plate given in Banks and others (1977), with compensation at the base of the lithosphere. The effective elastic thickness of the lithosphere typical of regions of continental extension is ~5 km (e.g., Bechtel and Forsyth, 1987; Barton and Wood, 1984). In the simple calculations below, we consider the problem in two dimensions (2-D). The deflection due to the removal of a water layer of thickness $u(x)$ is the inverse Fourier transform of

$$W(k) = U(k)R(k)$$

where $U(k)$ is the Fourier transform of $u(x)$, k is the wave number, and $R(k)$ is the isostatic response function given by

$$R(k) = -\frac{\rho_w g}{\rho_m g + Dk^4}$$

ρ_w and ρ_m are the densities of water and asthenospheric mantle (= 3.2 g/cm^3), g is the acceleration due to gravity, and D is the flexural rigidity given by $D = ET_e^3/12(1 - \sigma^2)$, where T_e is the effective elastic thickness of the lithosphere. We assume Young's modulus, $E = 7 \times 10^{10}$ Pa, and Poisson's ratio, $\sigma = 0.25$.

We investigated the effect of flexural isostasy on the altitude of the Dardanelles sill by considering a 2-D bathymetric profile across the Dardanelles, Gallipoli Peninsula, and Saros Gulf, perpendicular to the strike of the North Aegean Trough (Fig. 9a), and calculating the flexural isostatic uplift due to the removal of the water between sea level and a depth of 118 m (the depth to the lowest last glacial shorelines in the Aegean) for various elastic thicknesses (Fig. 9b). The 2-D bathymetric profile was chosen to be as representative as possible of the true three-dimensional water load in the vicinity of the profile. For elastic thicknesses of 2 km or more, the calculated level of the Dardanelles sill at the last lowstand is little different from its present-day altitude (−65 m); the small amount of uplift for elastic thicknesses of 5 km or more is due to the unloading of the Saros Gulf (Fig. 10c). The Dardanelles is a narrow (3–7 km) strait, so the additional 65-m-thick water load will be supported without local isostatic compensation for reasonable values of elastic thickness. The results of a similar analysis for a bathymetric profile across the Argolikos Gulf, where the −118 m glacial shoreline was observed by van Andel and Lianos (1984), indicate that Aegean sea level was below the level of the Dardanelles sill during the last lowstand whichever elastic thickness is assumed (Fig. 10a). This conclusion is still valid if the −118 m fossil shoreline in the Argolikos Gulf has tectonically subsided by 10 m since the end of the last glacial (Fig. 10b; based on an estimate for the return time of large normal faulting earthquakes, with a throw of 1 m, of ~10^3 yr).

It is therefore probable that the flow of marine water from the Aegean into the Sea of Marmara was precluded for at least part of the last glacial, and the level of the Sea of Marmara was then independent of Aegean sea level. Independent evidence of this comes from the shallow cores of Stanley and Blanpied (1980). They interpret the lower unit of one core, dated at 13 500 radiocarbon years B.P. (≈16 k.y. B.P. from Bard and others, 1990), as the deposits of an anaerobic, possibly saline lake. The core passes up into a unit containing rare planktonic foraminifera and coccoliths, which Stanley and Blanpied (1980) interpreted as lacustrine deposits with a limited marine influx.

Level of the Sea of Marmara During the Last Glacial

During the period when the Sea of Marmara was isolated from the Aegean, its level would have been controlled by the water balance and the contemporary level of the Dardanelles sill. If, in general, runoff exceeded evaporation in the Black Sea or Sea of Marmara regions, then a fluvial overflow would have existed through the Dardanelles strait, base level would be stable or gradually falling due to fluvial incision into the Dardanelles valley floor, and there would be a simple, monotonic progradation of deltaic deposits. Conversely, if evaporation exceeded runoff, then the buffering effect of the Dardanelles sill would not exist, and the lake level would be controlled by the water balance alone. For a relatively small basin like the Sea of Marmara, small variations in this balance would cause rapid changes in level and, consequently, the deltaic deposits would have a complex internal structure.

Direct evidence for former levels of the Sea of Marmara comes from the depths of the deltaic clinoform facies of stratigraphic unit B and other fossil shelf breaks (histogram in Fig. 11). The histogram has a strong concentration around −100 m, with a spread of ±10 m.

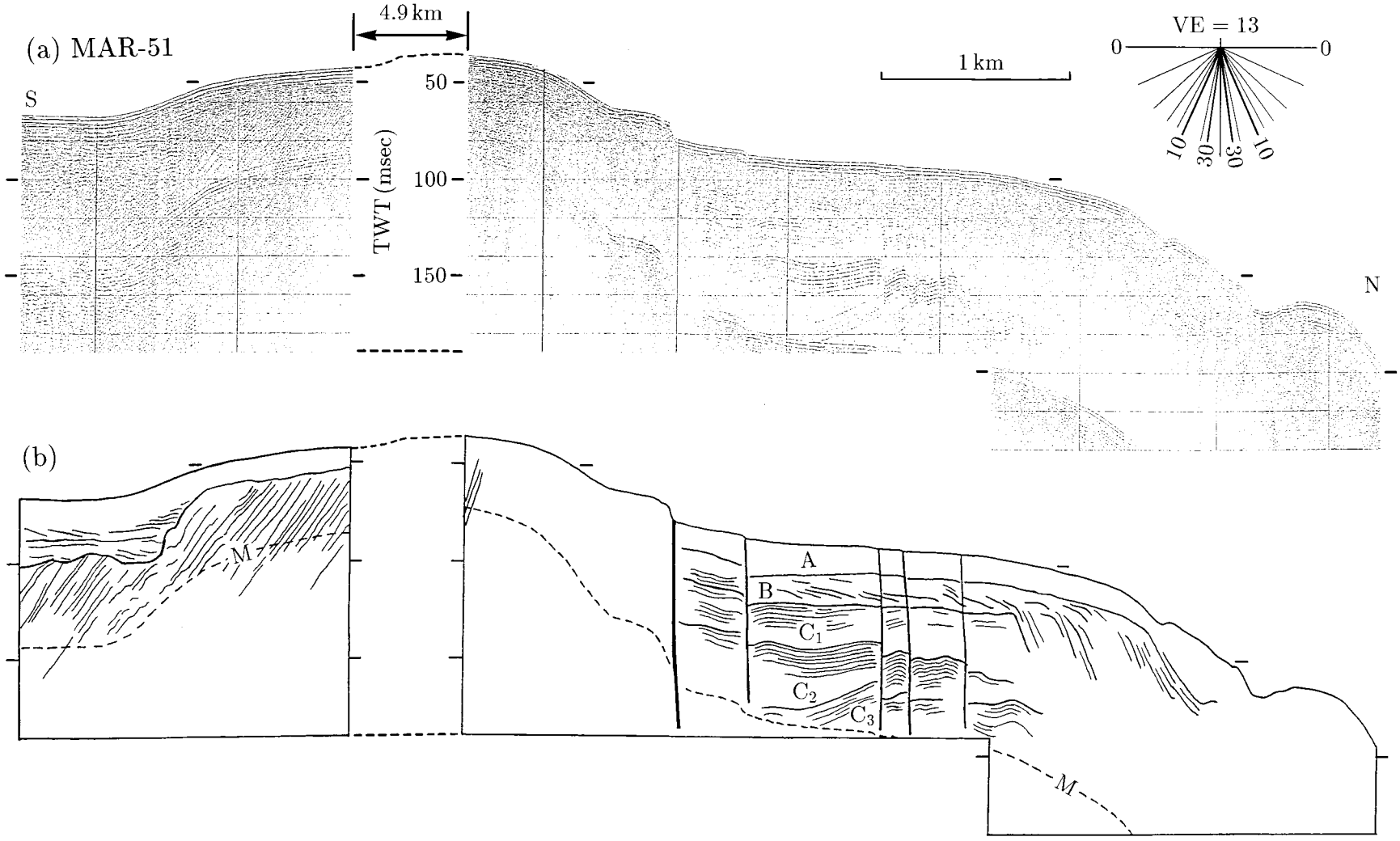

Figure 8. (a) Sparker profile MAR-51, immediately west of İmralı Island. For the location of the profile, see Figure 7d. (b) Interpretation of the sparker profile. The dashed line labeled M is the first sea-bed multiple; the letters A, B, C_1, C_2, and C_3 are the stratigraphic units defined in Figure 3.

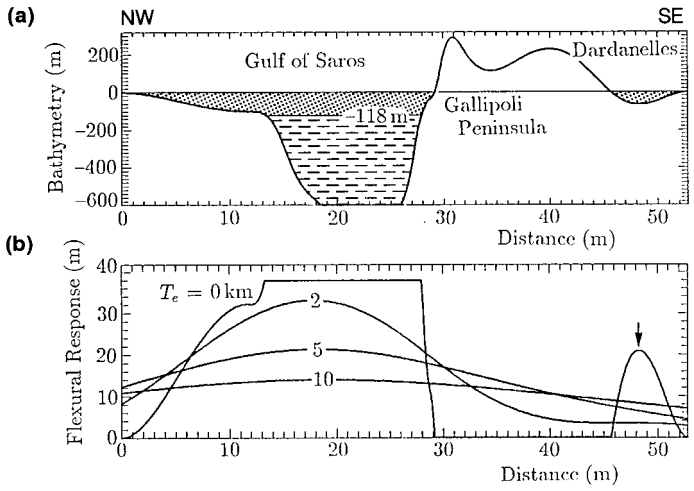

Figure 9. (a) Bathymetric profile across the Gulf of Saros, Gallipoli Peninsula, and Dardanelles, from 40 36 N, 26 11 E to 40 14 N, 26 33 E (see Fig. 1 for location). The hatched region is the 118 m relative sea-level rise since the last glacial lowstand in the Aegean (van Andel and Lianos, 1984). (b) The flexural isostatic response of the lithosphere along the profile in a, modeled as continuous elastic plates of various elastic thicknesses (T_e = 0, 2, 5, 10 km), to the removal of the distributed water load defined by the hachured region in a. The arrow marks the position of the Dardanelles sill and shows that for elastic thicknesses of more than 2 km, the altitude of the sill at the last glacial maximum differed little from that at present.

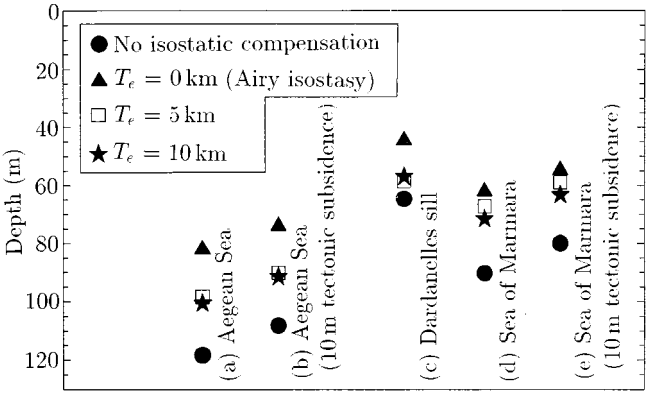

Figure 10. Estimates of the altitudes (relative to present-day sea level) of Aegean sea level, the Dardanelles sill, and the level of the Sea of Marmara during the last glacial lowstand. The values are obtained by calculating the flexural isostatic response of a lithospheric profile (modeled as a 2-D continuous elastic plate) to the removal of a distributed water load representing the postglacial sea-level rise. The different symbols, representing elastic plates of different thicknesses, are explained in the inset. (a) A profile from 37 20 N, 22 49 E to 37 44 N, 23 54 E, crossing the shelf break of the Argolikos Gulf where van Andel and Lianos (1984) observed glacial shorelines down to −118 m. (b) The same profile as (a), but the sea bed is assumed to have tectonically subsided by 10 m since the last glacial maximum. (c) A profile across the Dardanelles, described in Figure 9. (d) A north-south profile across the Sea of Marmara at longitude 28 30 E. A water layer of 90 m is removed, the estimated relative sea-level rise since the deposition of the latest clinoforms of stratigraphic unit B. (e) The same profile as (d), but the sea bed is assumed to have tectonically subsided by 10 m since the deposition of the clinoforms.

This peak includes all those profiles with the prograding clinoform facies. The spread of the peak may be due to differential subsidence (both tectonic and compactional) subsequent to deposition, differential isostatic response to the postglacial sea-level rise, or the shelf breaks not having formed at precisely the same time; for example, a delta lobe may have been abandoned before sea level reached its lowest position.

The Sea of Marmara is 70 km wide from north to south, and the shelf break of the broad southern shelf lies toward the center of the sea; therefore, the water-loaded subsidence at the shelf break, due to the postglacial sea-level rise, will approach the case of local isostatic compensation for an effective elastic thickness of the lithosphere of 5 km or less. Assuming the observed foreset-topset transition of the clinoforms at the shelf break making up stratigraphic unit B, now at −100 m, formed at a water depth of 10 m, and assuming no subsequent tectonic or compactional subsidence, then the relative sea-level rise is 90 m. Using the method previously described for the Dardanelles sill, we have estimated the flexural isostatic response of the southern shelf break of the central Sea of Marmara to the removal of a 90-m-thick water layer (Fig. 10d). For effective elastic thicknesses of 5 km or less, the estimated level of the Sea of Marmara contemporaneous with the deposition of the final clinoforms is close to the estimated altitude of the Dardanelles sill at the last lowstand, particularly if the clinoforms have undergone 10 m of subsequent tectonic or compactional subsidence (Fig. 10e). The clinoforms of stratigraphic unit B have a simple pattern of progradation, apparently controlled by a stable or gradual monotonic fall in base level. Therefore, we favor the hypothesis where the level of the Sea of Marmara was stabilized by an overflow across the Dardanelles during the deposition of stratigraphic unit B.

Pollen data from the north Aegean region indicate widespread *Artemisia* steppe vegetation during the last glacial maximum, generally thought to be characteristic of a cold, semiarid climate (van Zeist and Bottema, 1982). During the last glacial maximum there is some evidence for raised lake levels throughout the East Mediterranean region (Farrand, 1971; Prentice and others, 1992). Prentice and others (1992) attempted to reconcile these two apparently contradictory observations, suggesting a more seasonal climate with dry summers and cold wet winters. It is possible, therefore, that fluvial runoff into the Sea of Marmara exceeded evaporation from its surface, maintaining its level at the altitude of the Dardanelles sill. Another possibility, complementary with the first, is that an overflow existed across the Bosphorus during the last glacial maximum. Thiede (1974), using planktonic foraminifera, identified an influx of cool surface waters from the Aegean during the last glacial maximum (18 k.y. B.P.), attributed to meltwater from the Eurasian ice sheet flowing into the Aegean via the Caspian and Black Seas (Grosswald, 1980). In the Black Sea, shorelines from the last glacial maximum are found down to 80–90 m below present sea level (Shcherbakov and others, 1978), but this depth is uncorrected for isostatic effects due to the postglacial sea-level rise.

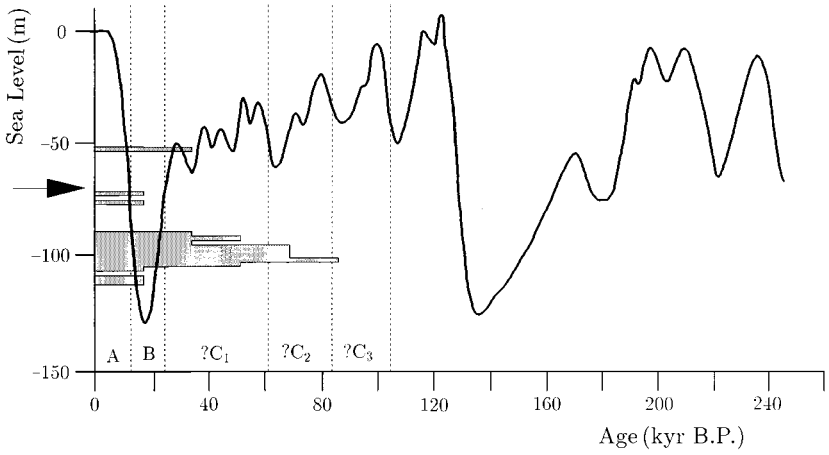

Figure 11. The sea-level curve for the Huon Peninsula (from Chappell and Shackleton, 1986) after correlation with oxygen isotope data. The histogram is the observed distribution with depth below present sea level of the altitude of the shelf break immediately prior to the deposition of stratigraphic unit A, the data being taken from sparker profiles. Where the prograding clinoform facies of stratigraphic unit B is present, it is the two-way time to the foreset-topset transition that is measured. Measurement error translates into a relative depth error of about 2 m. We assume a sea-water velocity of 1500 ms^{-1} and a surficial sediment velocity of 1750 ms^{-1}, although uncertainty in sediment velocity is not important because stratigraphic unit A is everywhere <10 m at the shelf break. The peak around −100 m includes all those profiles where the basinward-dipping, prograding clinoforms characteristic of stratigraphic unit B are observed, and in these cases it is the last position of the topset-foreset transition that is measured. The shallower shelf breaks are probably not of the same age. The arrow indicates the present sill depth of the Dardanelles strait. The dotted lines mark the tentative date ranges for the stratigraphic units described in this paper, which are based on our interpretation of the sparker profiles in terms of the sea-level curve.

Dating of Stratigraphic Units

The contact between stratigraphic units A and B is, in some sparker profiles, undulatory and mildly unconformable with the uppermost flat-lying unit draping the lower. We interpret stratigraphic unit A as a Holocene posttransgression marine deposit. The latest feasible and most probable date that the prograding clinoform facies of stratigraphic unit B could have been deposited was during the last glacial maximum and up to the early phase of deglaciation (25–13 k.y. B.P.) when the Sea of Marmara was isolated from the Aegean; this is the principal reason behind our dating of the unit.

Aksu and others (1987) described very similar deposits in the outer İzmir and Çandarlı Bays, offshore western Turkey. Their sparker profiles show stacked units of prograding clinoforms, which they interpreted as deltaics deposited during a falling sea level or lowstand. Radiocarbon dating of core material from the foresets of the unit underlying the present-day delta (Aksu and Piper, 1983) indicate that the clinoforms were deposited during the last major lowstand about 20 k.y. B.P.

Between 120 and 25 k.y. B.P., sea level had an overall decreasing trend with superposed oscillations; however, during this period sea level was always above −65 m (Fig. 11). Therefore, if the altitude of the Dardanelles sill were significantly different from today, then the Dardanelles would have been a marine strait, and the level of the Sea of Marmara would have been controlled by Aegean sea level. We tentatively interpret the reflection character of stratigraphic unit C in terms of sea-level oscillations. The strong reflectors bounding the subunits of stratigraphic unit C may be the expression of relatively coarser grained sediments, or minor unconformities formed during lowstands when the sea bed was above wave base. The transparent or weaker reflectors toward the lower part of each subunit may represent hemipelagic sediments deposited during highstands when the coastline was several kilometers south of the southern shelf break. A similar interpretation was invoked by Perissoratis and van Andel (1991) to explain alternating transparent and reflective units in the South Evvoikos Gulf, central Greece. If our interpretation of the alternating reflector strength within stratigraphic unit C is correct, then the periodicity of the subunits will be the same as the dominant frequency of the sea-level curve between 120 and 25 k.y. B.P. We use the high-amplitude oscillations with a frequency of ~20 k.y. in the sea-level curve to tentatively date the subunits within stratigraphic unit C (Fig. 11).

ACTIVE TECTONICS

The Sea of Marmara includes a series of tectonically active basins at the western end of the right-lateral North Anatolian fault (Şengör and others, 1985; Taymaz and others, 1991). In the vicinity of the Sea of Marmara, the surface faulting of the North Anatolian fault becomes distributed over an ~120 km broad zone (Barka and Kadinsky-Cade, 1988; Suzanne and others, 1990).

In this study, several major normal faults that cut surficial sediments were observed in the southern shelf east of Marmara Island (Fig. 12). One strikes along the northern coast of the Kapıdağ Peninsula; another is 11 km to the north; and a third strikes along the bathymetric escarpment north of İmralı Island. All of the observed faults strike approximately west-northwest–east-southeast and dip north. We infer that a major north-dipping normal fault strikes along the coast, from southeast of the Kapıdağ Peninsula to Gemlik Bay, where it links with the fault along the south shore of Lake İznik (Tanoğlu and Erinç, 1956). This coastal fault is evident from the geomorphology: The coastline between Bandırma and Gemlik is straight and in places high (Kara Dağ, 833 m; Fig. 1) with a steep coastal slope. Also TPAO multichannel profiles north of this coast have south-dipping reflectors.

The 6 October 1964 6.9 M_s Manyas earthquake was associated with surface breaks near Lake Manyas, 30 km south of the Sea of Marmara (Fig. 1; Ketin, 1966). This earthquake had an almost pure normal faulting mechanism (Taymaz and others, 1991) whose north-dipping nodal plane (the fault plane) strikes at 280°, subparallel to the observed offshore faults (Fig. 12). The fault pattern of the southern shelf region east of Marmara Island appears to be similar to that of the onshore region between Manyas and Bursa, to the south (Barka and Kadinsky-Cade, 1988). The faults of the southern shelf region east of Marmara Island clearly have large dip-slip normal

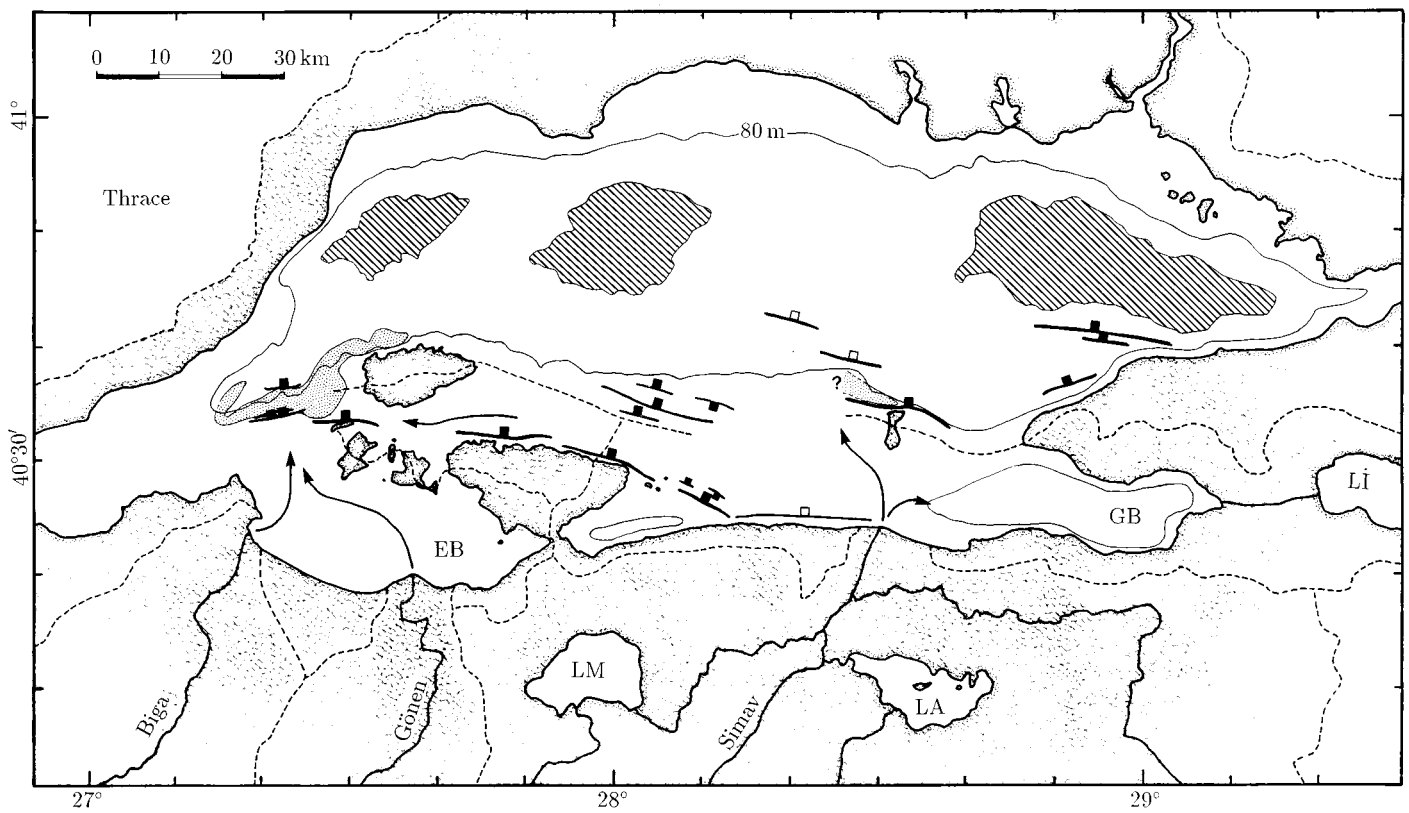

Figure 12. Paleogeography of the southern shelf during the last glacial maximum. Onshore, the solid lines represent the main river channels flowing into the Sea of Marmara, and the dashed lines are drainage divides. The drainage divides are extrapolated offshore onto the southern shelf assuming that the present-day bathymetry is an adequate approximation to the topography at the time. Offshore, the stippled area is the observed extent of the clinoform facies of stratigraphic unit B. The 80 m bathymetric contour is the estimated approximate coastline at the end of the deposition of stratigraphic unit B. Major basin-bounding faults in the southern shelf region are also shown; those we observed on seismic reflection profiles have filled blocks on their downthrown sides, whereas those inferred from other, indirect evidence have open blocks. Faults in the northern Sea of Marmara are not shown. The hachured areas are deep water basins, defined by the 1000 m bathymetric contour. LA, Lake Apolyont; Lİ, Lake İznik; LM, Lake Manyas; EB, Erdek Bay; GB, Gemlik Bay.

components, and because they have a similar strike to the Manyas earthquake fault plane, they may be almost pure normal faults.

SEDIMENT SUPPLY

The total catchment area of the Sea of Marmara is 39 290 km^2. In the Sea of Marmara, most rivers drain from the south: The drainage basin area to the south is more than six times that to the north. The southern drainage system is dominated by the catchments of the Simav, Gönen, and Biga Rivers (Fig. 12). The River Simav has a larger drainage basin (23 530 km^2) than the combined area of those of all other rivers flowing into the Sea of Marmara. The rivers of Thrace flow away from the Sea of Marmara and into the north Aegean. Therefore, the greater width of the shelf to the south of the Sea of Marmara may be explained, in part, by the much larger drainage network to the south. Because the tectonics of the southern shelf of the Sea of Marmara is dominated by approximately east-southeast–west-northwest–striking, north-dipping normal fault systems and associated half-graben basins, much sediment would be trapped in these basins. This occurs in the Simav drainage basin at present, where an extensive Holocene alluvial/lacustrine basin (including Lakes Manyas and Apolyont; Fig. 12) lies within the hanging walls of north-dipping normal faults between Manyas and Bursa (Barka and Kadinsky-Cade, 1988). The northern fault system appears to be more active, based on the greater depth of the northern basins; however, this impression will be exaggerated by the dominant sediment supply from the south.

All the sparker profiles across the southern shelf break, from the Şarköy subregion to the back-tilted terrace north of Marmara Island, have the prograding clinoform seismic facies characteristic of stratigraphic unit B, and the shelf break itself is delineated by the northern limit of the foreset progradation (Fig. 12). East of the Kapıdağ Peninsula, this facies was observed on only one profile (Fig. 8). From the sparker data, therefore, the volume of deltaic sediment of stratigraphic unit B appears to be greater west of Marmara Island than east of the Kapıdağ Peninsula, although this difference may be due to the poorer coverage by the sparker survey in the latter area. (Note the large area of shelf not traversed by sparker profiles between subregions [c] and [d] in Fig. 2.) If the observation is real, however, then it conflicts with the present-day drainage and fluxes of suspended sediment into these two areas, which is greater for the eastern area (Ergin and others, 1991).

If the level of the Sea of Marmara (relative to the sea bed) were about 80 m lower during the last glacial maximum, and assuming

that the morphology of the shelf has changed negligibly since that time, then the drainage basin of the Gönen and Biga rivers would have been significantly greater than today (Fig. 12). The region between the Kapıdağ Peninsula and Marmara Island, including Erdek Bay, would be drained by a river flowing west into the region of the extensive deltaic deposits observed on the sparker profiles. Sparker profiles about 4 km west of Marmara Island have features that may represent buried river valleys.

CONCLUSIONS

We interpret a unit of dipping reflectors on the sparker profiles (stratigraphic unit B) as the prograding clinoforms of a delta, deposited at a time when the level of the Sea of Marmara was significantly lower than it is at present and either at or below the level of the Dardanelles sill, so that flow of marine water into the Sea of Marmara was prevented. We argue that this unit was deposited during the last glacial maximum and early phase of deglaciation (25–13 k.y. B.P.), and we prefer the hypothesis that the level of the Sea of Marmara was stabilized by a fluvial overflow across the Dardanelles during this period to the alternative hypothesis that the level was controlled by water balance alone. Our preferred hypothesis is compatible with a through-flow of glacial meltwater from the Eurasian ice sheet by way of the Caspian and Black Seas.

We observed several active normal faults in the sparker data from the southern shelf of the Sea of Marmara, some of which have large displacements in coincident multichannel profiles and are associated with half grabens up to 3.0 s TWT deep. All the observed faults in the central southern shelf dip north and strike approximately west-northwest–east-southeast.

We partly attribute the greater width of the southern shelf compared to that of the north and the lack of significant fault scarps on the sea floor of the southern shelf to the much larger drainage basin area and greater sediment flux from the south. Sediment is likely to be trapped within the southern shelf by the west-northwest–east-southeast–striking normal fault systems and the associated half graben. This would exaggerate the apparent tectonic activity (inferred from the bathymetry) of the deep northern basins relative to the southern shelf.

ACKNOWLEDGMENTS

We thank the Hydrographic Department of the Turkish Navy for the opportunity to do this work, and the captain and crew of *T.C.G. Çubuklu* for the professional and efficient completion of the cruise. We also thank Celâl Şengör, who coordinated the cruise, and Muharrem Türkarslan and Süleyman Turgut of TPAO, who made available and helped interpret the multichannel data. Smith gratefully acknowledges sponsorship from British Petroleum. Taymaz thanks the Turkish Ministry of Higher Education for sponsorship during his Ph.D. work. We also thank Tjeerd van Andel and referees Stephen Lewis and Jill McCarthy for their useful and constructive comments.

REFERENCES CITED

Aksu, A. E., and Piper, D. J. W., 1983, Progradation of the late Quaternary Gediz delta, Turkey: Marine Geology, v. 54, p. 1–25.
Aksu, A. E., Piper, D. J. W., and Konuk, T., 1987, Late Quaternary tectonic and sedimentary history of outer Izmir and Candarli Bays, western Turkey: Marine Geology, v. 76, p. 89–104.
Ambraseys, N. N., 1988, Engineering seismology: Earthquake Engineering and Structural Dynamics, v. 17, p. 1–105.
Ambraseys, N. N., and Finkel, C. F., 1991, Long-term seismicity of Istanbul and of the Marmara Sea region: Terra Nova, v. 3, p. 527–539.
Banks, R. J., Parker, R. L., and Huestis, S. P., 1977, Isostatic compensation on a continental scale: Local versus regional mechanisms: Geophysical Journal of the Royal Astronomical Society, v. 51, p. 431–452.
Bard, E., Hamelin, B., Fairbanks, R. G., and Zindler, A., 1990, Calibration of ^{14}C over the last 30,000 years using U/Th ages obtained by mass spectrometry on Barbados coral: Nature, v. 345, p. 405–410.
Barka, A. A., and Kadinsky-Cade, K., 1988, Strike-slip fault geometry in Turkey and its influence on earthquake activity: Tectonics, v. 3, p. 663–684.
Barton, P., and Wood, R., 1984, Tectonic evolution of the North Sea Basin: Crustal stretching and subsidence: Geophysical Journal of the Royal Astronomical Society, v. 79, p. 987–1022.
Bechtel, T. D., and Forsyth, D. W., 1987, Isostatic compensation in the Basin and Range, USA: Eos (Transactions, American Geophysical Union), v. 44, p. 1450.
Chappell, J., and Shackleton, N. J., 1986, Oxygen isotopes and sea level: Nature, v. 324, p. 137–140.
Ergin, M., Bodur, M. N., and Ediger, V., 1991, Distribution of surficial shelf sediments in the northeastern and southwestern parts of the Sea of Marmara: Strait and canyon regimes of the Dardanelles and Bosphorus: Marine Geology, v. 96, p. 313–340.
Fairbanks, R. G., 1989, A 17,000-year glacio-eustatic sea level record: Influence of glacial melting rates on the Younger Dryas event and deep-ocean circulation: Nature, v. 342, p. 637–642.
Farrand, W. R., 1971, Late Quaternary paleoclimates of the eastern Mediterranean area, *in* Turekian, K. K., ed., The late Cenozoic glacial ages: New Haven, Connecticut, Yale University Press, p. 727–741.
Grosswald, M. G., 1980, Late Weichselian ice sheet of northern Eurasia: Quaternary Research, v. 13, p. 1–32.
IOC-UNESCO, 1981, International bathymetric chart of the Mediterranean: Leningrad, USSR, Ministry of Defence, 10 sheets, scale 1:1 000 000.
Ketin, I., 1966, 6 Ekim 1964 Manyas depremi esnasında zeminde meydana gelen tansiyon çatlakları: Türkiye Jeoloji Kurumu Bülteni, v. 10, p. 44–51.
Lambeck, K., Johnston, P., and Nakada, M., 1990, Holocene glacial rebound and sea-level change in NW Europe: Geophysical Journal International, v. 103 p. 451–468.
Maden Tetkik ve Arama Enstitüsü (M.T.A.), 1964, Geological map of Turkey, 1:500,000 Istanbul sheet: Ankara, Turkey, Institute of Mineral Research and Exploration.
Perissoratis, C., and van Andel, T. H., 1991, Sea-level changes and tectonics in the Quaternary extensional basin of the South Evvoikos Gulf, Greece: Terra Nova, v. 3, p. 294–302.
Prentice, I. C., Guiot, J., and Harrison, S. P., 1992, Mediterranean vegetation, lake levels and palaeoclimate at the Last Glacial Maximum: Nature, v. 360, p. 658–660.
Schrader, H.-J., 1979, Quaternary paleoclimatology of the Black Sea basin: Sedimentary Geology, v. 23, p. 165–180.
Şengör, A. M. C., Görür, N., and Şaroğlu, F., 1985, Strike-slip faulting and related basin formation in zones of tectonic escape: Turkey as a case study, *in* Biddle, K. T., and Christie-Blick, N., eds., Strike-slip deformation, basin formation and sedimentation: Society of Economic Paleontologists and Mineralogists Special Publication, v. 37, p. 227–264.
Shcherbakov, F. A., Kuprin, P. N., Potapova, L. I., Polyakov, A. S., Zabelina, E. K., and Sorokin, V. M., 1978, Sedimentation on the continental shelf of the Black Sea: Moscow, USSR, Nauka Press, 210 p.
Stanley, D. J., and Blanpied, C., 1980, Late Quaternary water exchange between the eastern Mediterranean and the Black Sea: Nature, v. 285, p. 537–541.
Suzanne, P., Lyberis, N., Chorowicz, J., Nurlu, M., Yurur, T., and Kasapoglu, E., 1990, La géométrie de la faille norde-anatolienne à partir d'images Landsat-MSS: Bulletin de la Société Géologique de France, v. 8, p. 589–599.
Tanoğlu, A., and Erinç, S., 1956, The Garsak Gorge and the Sakarya River diversion: Review of the Geographical Institute of the University of Istanbul, v. 3, p. 1–12.
Taymaz, T., Jackson, J. A., and McKenzie, D. P., 1991, Active tectonics of the north and central Aegean Sea: Geophysical Journal International, v. 106, p. 433–490.
Thiede, J., 1974, A glacial Mediterranean: Nature, v. 276, p. 680–683.
Tushingham, A. M., and Peltier, W. R., 1992, Validation of the ICE-3G Model of Würm-Wisconsin deglaciation using a global data base of relative sea level histories: Journal of Geophysical Research, v. 97, p. 3285–3304.
van Andel, T. H., and Lianos, N., 1984, High-resolution seismic reflection profiles for the reconstruction of postglacial transgressive shorelines: An example from Greece: Quaternary Research, v. 22, p. 31–45.
van Zeist, W., and Bottema, S., 1982, Vegetational history of the eastern Mediterranean and the Near East during the last 20,000 years, *in* Bintliff, J. L., and van Zeist, W., eds., Palaeoclimates, palaeoenvironments and human communities in the eastern Mediterranean region in later prehistory: British Archaeological Reports, International Series, v. 133, p. 277–321.

Manuscript Received by the Society December 28, 1992
Revised Manuscript Received January 26, 1995
Manuscript Accepted February 6, 1995
Cambridge Earth Sciences Contribution No. 4289

Printed in U.S.A.